IPP-Report

IPP Max-Planck-Institut für Plasmaphysik

P. J. McCarthy, P. Martin, W. Schneider

# The CLISTE Interpretive Equilibrium Code



IPP 5/85
Mai 1999

**Abstract**

The CLISTE interpretive equilibrium code solves the Grad-Shafranov equation for regularized source profiles under the constraint that a least squares fit to a set of experimental signals is obtained. The code developed from the Garching Equilibrium Code, whose functionality has been extended to enable predictive or interpretive modes of operation. CLISTE can run in a comprehensive slow mode where the measurements may depend nonlinearly on the free parameters, or a more restricted fast mode (whose algorithm is similar to that of the well-known EFIT code) where the relationship between free parameters and measurements must be linear. Novel features of the code include the ability to handle scrape-off layer currents (assuming ideal MHD force balance) and confidence band calculations for profile quantities. Results are illustrated by a sample ASDEX Upgrade equilibrium.

# Contents

# CLISTE Code

**P. J. Mc Carthy, P. Martin, W. Schneider**

## 1 Overview

CLISTE [1] is an acronym for CompLete Interpretive Suite for Tokamak Equilibria. The CLISTE code finds a numerical solution to the Grad-Shafranov equation [1, 2]

$$-\left(\frac{\partial^2\psi}{\partial R^2}-\frac{1}{R}\frac{\partial\psi}{\partial R}+\frac{\partial^2\psi}{\partial Z^2}\right) = \mu_o R^2 p'(\psi)+FF'(\psi) \equiv \mu_o R j_\phi \quad (1)$$

for a given set of poloidal field coil currents and limiter structures by varying the free parameters in the parameterization of the $p'(\psi)$ and $FF'(\psi)$ source profiles which define the toroidal current density profile $j_\phi$ so as to obtain a best fit in the least squares sense to a set of experimental measurements. These measurements can include external magnetic data, MSE data, kinetic data, $q$-profile information from SXR measurements, etc., and the free parameters are varied such that the penalty or *cost function*, i.e. the squared modulus of the vector of (weighted) differences between the set of experimental measurements and those predicted by the equilibrium solution, is minimized.

The code proceeds by two distinct and user-selectable algorithmic paths. The older algorithm, which is by far the slowest, allows source profile parameterizations which may be nonlinear in the free parameters, e.g. $p'(\psi) \propto \psi^a$ where $a$ is to be determined. The newer 'Fast Mode' algorithm, which is similar to that used in the well-known EFIT code, is restricted to source profiles which are linear in the free parameters. Both algorithms are described below.

## 2 The Slow Mode

Here, CLISTE calls the Garching Equilibrium Code [3] (GEC) iteratively with the goal of finding an ideal MHD equilibrium for which a user-specified set of diagnostic signals best matches (in a least-squares sense) the corresponding set of experimental values. The optimization is carried out by the nonlinear least squares optimization routine E04FCF from the NAG library. [4] For each calculation of the cost function required by E04FCF, the GEC is called to calculate a predictive equilibrium using the latest set of free parameters.

The GEC, which is used both to generate equilibrium databases for function parameterization (FP) purposes and also for CLISTE runs, has the following data/algorithmic features particular to ASDEX Upgrade:

Up to 18 conductor groups may influence the equilibrium. These consist of the following poloidal field coils: IV1o, IV1u, IV2o, IV2u, IV3o, IV3u, IPslo, IPslu, ICoIo, ICoIu, IOHo, IOHu, IOH2od, IOH2ud, PslQo, PslQu, Psl3o, Psl3u. The OHo/OHu division is artificial since the two currents are constrained to be equal (the division is necessitated by the large number of windings in the solenoid). The following current groups are passive currents for which there are no Rogowski coils, but which have a clear influence on certain close-lying measurements: PslQo/u are the 150 ms 'quadrupole' PSL modes which have a cosine-like spatial dependence

[1] *klish-teh*, Gaelic for clever

along the longer (30 cm) axis of each arm of the passive conductor (PSL). Psl3o/u are even more localized *circa* 20 ms modes which vary along the shorter (8 cm) axis of each PSL arm. So far, these unmeasured current groups have not been allowed to vary (they are expected to be significant only during fast current ramps or plasma movements).

The constraints on the conductor currents are as follows: All conductor currents are read in as input data by the GEC. For FP equilibrium database generation, these are usually chosen randomly. For CLISTE runs, the experimental coil currents are read in. Among other input data, the R and Z coordinates of the magnetic axis are also read in. In the case of CLISTE the parameters Rmag and Zmag, already recovered from magnetic data by the standard function parameterization package 'FPG', are used as initial guesses. The GEC must honour the input magnetic axis position to ensure stability of the convergence algorithm. This is achieved by allowing the IV2o and IV2u coil currents to vary so that the R and Z components of the poloidal field vanish at the prescribed magnetic axis position. Thus the input IV2o, IV2u currents are ignored for each predictive equilibrium calculation. However, IV2o and IV2u are included in the cost function so that CLISTE will vary (Rmag,Zmag) during successive calls to GEC to minimize the difference with respect to experiment of the final IV2o, IV2u values. (There is one exception to this, namely when the (Rmag,Zmag) parameters themselves are included in the cost function. This occurs when an 'FPG equilibrium' is sought: see below.) The conditions on the coil currents are solved in the subroutine XCUR10.

## 2.1 Current profile parameterization in the Slow Mode

The toroidal current density profile in the 'Slow Mode' is parameterized by the coefficients, $a_p, b_p, c_p, d_p, g_p, h_p$, $a_f, b_f, c_f, d_f, g_f, h_f$, and $sol_p, sol_f, pol_p, pol_f$, such that

$$j_\phi = C_{p'} R \underbrace{\hat{\psi}^{a_p}\left(e^{b_p x + c_p x^2 + d_p x^3} + g_p e^{-(h_p\hat{\psi})^2}\right)}_{\hat{p}'(\psi)} + \frac{C_{FF'}}{R}\underbrace{\hat{\psi}^{a_f}\left(e^{b_f x + c_f x^2 + d_f x^3} + g_f e^{-(h_f\hat{\psi})^2}\right)}_{\hat{f}\hat{f}'(\psi)} \quad (2)$$

where $\hat{\psi}$ is unity on the magnetic axis, zero on a surface near the plasma boundary whose location is determined by the $sol_p, sol_f, pol_p, pol_f$ parameters (see below), and $x = 1 - \hat{\psi}$. The scale factors $C_{p'}$ and $C_{FF'}$, which are output parameters, determine the overall toroidal current driven by the $p'$ and $FF'$ terms, respectively, as well as the poloidal beta $\beta_{pol}$.

The structure of the $\hat{p}'(\psi)$ and $\hat{f}\hat{f}'(\psi)$ terms is symmetric and consists of (i) a bulk plasma term comprising a simple power law $\hat{\psi}^a$ modulated by an exponentiated cubic polynomial $e^{b\,x + c\,x^2 + d\,x^3}$ and (ii) a bootstrap term $\hat{\psi}^a \times g\, e^{-(h\hat{\psi})^2}$ which is localized to the edge region when $h^2 \gg 1$.

The GEC has recently been extended to allow scrape-off layer (SOL) currents in the equilbrium calculations under the assumption that $\mathbf{J} \times \mathbf{B} = \nabla p$ also holds in the SOL. The current density is truncated where the open field lines intersect material structures, the possible effects on the equilibrium of the return currents through the material structures being neglected. The depth of the SOL is independently selectable for the $p'$ and $FF'$ source terms, and for each of $p'$ and $FF'$ there are furthermore two SOL depths to be specified, one for the public and one for the private flux regions. The SOL depth in Vs for the $p'$ term is

$$dsol_p = sol_p \times 0.2\pi R_o I_p$$

where $R_o = 1.65\,\mathrm{m}$ is the ASDEX Upgrade reference major radius, $I_p$ is the plasma current in $MA$, and $0.2\pi R_o I_p$ is the magnetic axis - plasma boundary flux difference (in $Vs$) for a circular, straight cylinder, flat plasma current distribution of length $2\pi R_o$. (This choice of scaling ensures $dsol_p$ is independent of the shape of the current profile.) Thus the input parameter $sol_p$ is to

be interpreted as the fraction of this flux difference which defines the (magnetic) depth of the $p'$ term contribution to the SOL current density. It should therefore be valued at the order of 1% (e.g. $sol_p = 0.01$). The depth of the $p'$ term in the private flux region(s) is specified by the parameter $pol_p$. This is interpreted as a fraction of the corresponding public region depth. Thus, if $dpol_p$ is the depth in Vs, then $dpol_p$ is calculated using the formula

$$dpol_p = pol_p \times dsol_p$$

where $dsol_p$ is the depth, in Vs, in the public region, as defined above. The equivalent definitions for the $FF'$ terms are identical to those for the $p'$, except that the $sol_p$ and $pol_p$ input parameters are replaced by $sol_f$ and $pol_f$, respectively.

The normalized source profiles $\hat{p}'(\psi), \hat{FF}'(\psi)$ and their respective integrals $\hat{p}(\psi), \hat{f}^2(\psi)/2$ are calculated on a 1001 point 1-D grid in the data input subroutine DEFPAR. The array names are PYAGD, FFYAGD, PYAG, FFYAG. The current density profile is updated in subroutine CURFY.

## 2.2 Short Description of subroutines called by CLISTE in the Slow Mode

**SMAINB**: Main subroutine of GEC.

**lsqDUP**: Initializes a flag in a DUPlicate shell version of the user-specified routine LSQFUN (see below).

**E04FCF**: A comprehensive nonlinear least squares optimization NAG routine which does not require analytic derivatives of the cost function with respect to the free parameters. E04FCF is normally called once per CLISTE run. However, if any coil currents other than IV2o, IV2u are allowed to vary (this option is rarely exercised), there is a second, 'preliminary' E04FCF call with a restricted current profile consisting of just 2 shape parameters (one each for the $p'$ and $FF'$ profiles). The resulting output coil current values (other than IV2o, IV2u) are then frozen for the main E04FCF call, where all current density profile parameters specified by the input data, including possible SOL currents, are allowed to vary. The cost function J is specified in the user-supplied subroutine LSQFUN, which is called internally from E04FCF

**LSQFUN**: This routine is called by the NAG nonlinear least squares optimization routine E04FCF, which solves the optimization problem in CLISTE. LSQFUN is by far the largest CLISTE-specific subroutine (1400 lines, excluding commons) but its function is very simple: It calls the GEC with the latest set of free parameter values and then builds the cost function J. This consists of calculating individual residuals which are differences between GEC-predicted signals and the corresponding experimental values which have been read in in the main CLISTE program and are passed via the common array SIGARR. The k'th residual is multiplied by its weighted include flag WINCL(k). If WINCL(k)=0 then this signal does not contribute to the cost function.

The signal groups currently admitted to the cost function calculation are:

(i) 0 – 17 in-vessel flux differences

(ii) 0 – 51 in-vessel magnetic field measurements (38 tangential, 13 normal)

(iii) 0 – 12 coil currents

(iv) 0 – 17 flux differences outside the vacuum vessel.

(v) 0–16 field measurements outside the vacuum vessel (these are poorly calibrated and therefore not recommended at present)

(vi) 0 – 30 FPG parameters. Choosing to construct the cost function from these parameters alone, instructs CLISTE to find the equilibrium most compatible with the selected FPG parameters.

(vii) 0 – 16 pressure measurements at 16 vertical YAG channels at $R = 1.78$. The pressures are calculated in subroutine PRESID.

(viii) The mid-plane radius of the $q = 1$ surface from SXR. The flux surface with this radius is determined in subroutine SXRCAL, and hence the corresponding $q$ value, whose deviation from unity defines the residual.

(ix) 0 – 11 MSE channels. The quantity

$$\tan\gamma_m = \frac{A(1)B_r + A(2)B_t + A(3)B_z + A(4)E_r/v_{beam}}{A(5)B_r + A(6)B_t + A(7)B_z + A(8)E_r/v_{beam} + A(9)E_z/v_{beam}}$$

is calculated for each channel in subroutine MSECAL using fixed numerical coefficients A(1-9) provided by R. Wolf. The radial electric field is inferred from spectroscopic measurements of toroidal and poloidal rotation velocities. $\tan\gamma_m$ is the quantity directly measured by the MSE diagnostic.

**E04YCF**: This is an auxiliary NAG routine to calculate the variance-covariance error matrix for the free (equilibrium) parameters in the cost function optimized by E04FCF. This matrix, 'Vmat', is repeatedly used to calculate the error bars for equilibrium parameters which are not explicitly fitted as follows:

$$\sigma(g) = \sqrt{\nabla^t g \cdot \mathbf{Vmat} \cdot \nabla g}$$

where $\nabla g$ is the gradient of the parameter $g$ with respect to the vector of fitted parameters. $\nabla g$ is obtained numerically by varying each of the fitted parameters in turn about its solution value, calling GEC and noting the difference in the output value of $g$ with respect to the solution value.

**RHOMCAL**: Calculates $\rho_{mid}(R)$ along the horizontal plane $Z = Z_{mag}$ where $\rho_{mid}$ is the normalized 'mid-plane' diameter of the flux surface intersecting the point $R, Z_{mag}$. $\rho_{mid}$ is calculated for $R = 1.01,\ 1.02, \cdots, 1.20$m and stored in the common array RHOMIDA. More precisely we have, for $R < R_{mag}$ (with an equivalent expression for the case $R > R_{mag}$)

$$\rho_{mid}(R) = \frac{R_{out}(R) - R}{R_{P,out} - R_{P,in}}$$

where $R_{out}(R)$ is the corresponding $R > R_{mag}$ point where the flux contour intersecting $(R, Z_{mag})$ again intersects the horizontal line $Z = Z_{mag}$, and $(R_{P,in}, R_{P,out})$ are the points where the plasma boundary cross section intersects $Z = Z_{mag}$. This array properly belongs within GEC, but was first added as part of the development of CLISTE.

**QMCAL**: Calculates $q(R)$ in the same spirit as $\rho_{mid}$ above.

**G05EAF, G05EZF**: The input parameter ICONF specifies whether confidence bands for the $p(R)$, $q(R)$, $j(R)$ etc. 'mid-plane' profiles are to be calculated by Monte Carlo methods (ICONF=1) or 'analytically' (ICONF=2). ICONF=2 is normal. To test the integrity of the analytical calculation, however, occasionally ICONF=1 is used. In this case, the random values of the vector of fitted parameters are selected from a multinormal distribution with a variance-covariance matrix identical, within an input-specified scale factor (VSCFAC), to the matrix 'Vmat' (see above). G05EAF is a 'set-up' routine and G05EZF generates (pseudo-)random parameter vectors.

**F06PAF**: NAG matrix-vetor multiplication routine. Carries out calculations of the form $\nabla^t g \cdot \mathbf{Vmat}$ etc.

**eqDSKw**: On successful convergence to a solution, writes the CLISTE equilibrium flux function to disk.

### 2.3 Timing issues in the Slow Mode

The Slow Mode algorithm requires the order of 1 minute or more (increasing with the number of free parameters in the source function parameterization) on a 300 MHz Sun sparc ultra workstation. Each call to the user-defined subroutine LSQFUN by E04FCF, using the latest values for the free parameters as chosen by the search algorithm in E04FCF, requires a full equilibrium calculation by GEC which consumes *circa* 1 second of CPU time for a $65 \times 129$ computational grid. The GEC calculation is itself an iterative process where the Poisson-like equation

$$-\left(\frac{\partial^2\psi}{\partial R^2} - \frac{1}{R}\frac{\partial\psi}{\partial R} + \frac{\partial^2\psi}{\partial Z^2}\right) = \mu_o R j_\phi(R,Z) \qquad (3)$$

is solved for a given $j_\phi(R,Z)$ prescribed by the free parameters and the latest flux surface topology. The $p'(\psi)$ and $FF'(\psi)$ profile coefficients are fixed during the GEC convergence process and only the flux grid is iterated. Thus any change in the profile coefficients requires another full equilibrium calculation which is computationally expensive.

## 3 The Fast Mode

The optimization algorithm would be speeded up considerably were it possible to vary the $p'(\psi)$ and $FF'(\psi)$ coefficients simultaneously with the grid of poloidal flux values. Such an algorithm forms the kernel of the optimization procedure used in the EFIT interpretive equilibrium code. [6, 7] A critical requirement for the practical success of the algorithm is that all diagnostic signals contributing to the cost function be linear in the free parameters. When this holds, it is possible to determine the optimum values of the free parameters for a given grid of flux values by a *linear regression.* (There is no reason why a nonlinear optimization would not work here also, except that it would once again lead to longer execution times – though not on the scale of the Slow Mode time requirements discussed above because here we would still find a solution based on a single converged equilibrium). Note this does not mean, as a superficial reading of the EFIT literature might sometimes suggest, that the entire problem has been linearized, since the iteration of the poloidal flux grid following each (linear) optimization of the free parameters is an intrinsically nonlinear process. The linearity requirement means that $j_\phi$ itself, and hence the $p'(\psi)$ and $FF'(\psi)$ source profiles must also be linear in the free parameters, as is apparent from Eq. (3). We have implemented the essentials of this idea by devising a new convergence algorithm for the GEC with the following features:

(i) The stabilization of the plasma position during convergence that was previously provided by fixing the coordinates of the magnetic axis is now achieved by adding the vertical position of the plasma as an additional auxiliary free parameter to the linear regression problem solved at each cycle of the convergence process. When the equilibrium converges properly, the final value of this vertical shift parameter is typically the order of 0.1 mm, i.e. negligible. One consequence of this change is that the 'correction currents', in our case the IV2o and IV2u coil currents, used to conserve the magnetic axis position in the standard GEC algorithm are no longer needed (the

vertical shift parameter can be interpreted as an artifical radial field produced by an appropriate combination of correction currents with one degree of freedom). The axis position itself no longer plays an explicit role in the convergence algorithm.

(ii) During each iteration cycle, a linear optimization of the free parameters in the $p'(\psi)$ and $FF'(\psi)$ profiles is carried out as follows: Let the linear parameterization of the source profiles be given by

$$\begin{aligned} p'(\psi) &= \sum_{i=1}^{m_p} c_i \, \pi_i(\psi) \\ FF'(\psi) &= \sum_{j=1}^{m_{FF}} d_j \, \varphi_j(\psi) \end{aligned} \tag{4}$$

where $\pi_i(\psi)$ and $\varphi_j(\psi)$ are arbitrary functions of $\psi$ with fixed coefficients and $c_i$, $d_j$ are the free parameters in the problem. Thus $\pi_i(\psi)$ and $\varphi_j(\psi)$ constitute the basis functions of the plasma current distribution where $\psi$ is the full equilibrium flux function from the previous iteration cycle. We now generate corresponding poloidal flux basis functions $\psi_{p,i}^{new}$ and $\psi_{FF,j}^{new}$ with which we will construct the updated equilibrium flux function by solving the 'Poisson problem'

$$\begin{aligned} -\left( \frac{\partial^2 \psi_{p,i}^{new}}{\partial R^2} - \frac{1}{R} \frac{\partial \psi_{p,i}^{new}}{\partial R} + \frac{\partial^2 \psi_{p,i}^{new}}{\partial Z^2} \right) &= \mu_o R^2 \pi_i(\psi) \qquad (p'(\psi) \text{ terms}) \\ -\left( \frac{\partial^2 \psi_{FF,j}^{new}}{\partial R^2} - \frac{1}{R} \frac{\partial \psi_{FF,j}^{new}}{\partial R} + \frac{\partial^2 \psi_{FF,j}^{new}}{\partial Z^2} \right) &= \varphi_j(\psi) \qquad (FF'(\psi) \text{ terms}) \end{aligned} \tag{5}$$

separately for each $\psi_{p,i}^{new}$ and $\psi_{FF,j}^{new}$. Note that Eq. (5) takes care only of that part of the updated equilibrium flux generated by the plasma current distribution. The full equilibrium flux also includes the contribution from the external measured currents, none of which are allowed to vary in the Fast Mode. In terms of the as yet undetermined coefficients $\{c_i\}$ and $\{d_j\}$, the updated full equilibrium flux is given by

$$\psi^{new} = \sum_{i=1}^{m_p} c_i \, \psi_{p,i}^{new} + \sum_{j=1}^{m_{FF}} d_j \, \psi_{FF,j}^{new} + \psi^{ext} \tag{6}$$

The solution grids for $\psi_{p,i}^{new}$ and $\psi_{FF,j}^{new}$ yielded by Eq. (5), which are just the plasma flux basis functions for each unit strength $j_\phi$ basis function, are passed individually to the routine which calculates the predicted measurements from the flux function. In this way, we construct a matrix of $m_p + m_{FF}$ columns of 'basis values' $b_{n,k}$, $((n=1,\ldots,N_m),\ k=1,\ldots,m_p+m_{FF})$ for each of $N_m$ measurements. The value of $b_{n,k}$ is the contribution to the $n$th measurement prediction per unit strength of the $k$th basis function. An extra column catering for the vertical shift parameter is added to the matrix by calculating the change in each measurement (again using the full $\psi$ function from the previous iteration) when its $Z$ position is shifted by $-1\,\mathrm{cm}$. This gives the sensitivity per $+1\mathrm{cm}$ shift in the plasma vertical position. An additional row is added to the matrix for each regularization condition on the free parameters. This will be discussed below. If $\mathbf{B}$ is the data matrix as just described, and $\mathbf{y}$ is the vector of measurements less all contributions from measured external currents, then the optimization problem reduces to solving the linear regression

$$\mathbf{y} = \mathbf{B} \cdot \boldsymbol{\alpha} \tag{7}$$

where $\boldsymbol{\alpha}$ is the solution vector of optimized free parameters for the present iteration cycle. The equation for $y_n$ in the overdetermined system of linear equations which constitutes the linear

regression problem is thus

$$y_n = \sum_{k=1}^{m_p+m_{FF}+1} \alpha_k \, b_{n,k}$$
$$\equiv \sum_{i=1}^{m_p} c_i \, b_{n,i} + \sum_{j=1}^{m_{FF}} d_j \, b_{n,m_p+j} + \Delta Z \times b_{n,m_p+m_{FF}+1} \quad (8)$$

Once $\boldsymbol{\alpha}$ has been determined, we proceed to construct the updated full equilibrium flux grid. We first compute the updated plasma flux function $\psi_{plas}$ by once more solving Eq. (3) where the right-hand side now is the full $\mu_o j_\phi$ profile constructed from the first $m_p + m_{FF}$ elements of the newly obtained $\boldsymbol{\alpha}$ vector:

$$-\left(\frac{\partial^2 \psi_{plas}}{\partial R^2} - \frac{1}{R}\frac{\partial \psi_{plas}}{\partial R} + \frac{\partial^2 \psi_{plas}}{\partial Z^2}\right) = \mu_o R^2 \sum_{i=1}^{m_p} c_i \, \pi_i(\psi) + \sum_{j=1}^{m_{FF}} d_j \, \varphi_j(\psi) \quad (9)$$

(This step is necessary because the individual basis function flux grids were not stored.) Finally, the external flux contribution $\psi_{ext.}$ (i.e. the summed contributions from measured currents) is restored to yield $\psi^{new} = \psi_{plas} + \psi_{ext.}$. The entire procedure is iterated until a user-specified convergence criterion is satisfied. Due to the omission of the vertical shift parameter from Eq. (9), the solution method is not rigorously consistent; however as already noted earlier, the typical value of the shift for a properly converged equilibrium is *circa* 0.1 mm, which is quite negligible.

### 3.1 Current profile parameterization in the Fast Mode

The linear parameterization of the current profile required by the Fast Mode has been implemented in the form of a cubic spline representation in terms of the flux label $x : 0 \leq x \leq 1$ where $x = 1 - \hat{\psi}$ is zero at the magnetic axis and unity near the plasma boundary (the precise location is determined by the values of $dsol_p$ and $dsol_f$ - see corresponding subsection on the Slow Mode above). There are up to six internal knots for both the $p'(\psi)$ and $FF'(\psi)$ source profiles. The number ($\leq 6$) and positions of the knots are user-selectable, but are then fixed during optimization. The profile values at the knot locations constitute the set of free parameters. Together with an edge knot at the magnetic axis ($x = 0$) whose value is always free, a zero-valued knot at $x = 1$ and 'natural spline' (i.e. zero curvature) end conditions, this amounts to a maximum of 14 free parameters, corresponding in number to the 12 profile shape parameters and 2 profile magnitude parameters ($C_{p'}$, $C_{FF'}$) in Eq. (2) for the Slow Mode. The relationship between the SOL depth parameters and the cost function is nonlinear, hence these have to be fixed in the case of the Fast Mode. This is not a severe constraint, since allowing these parameters to vary in the Slow Mode has not worked out well in practice, and in both slow and fast modes where an optimization of these parameters is desired, the most practical approach is to make separate CLISTE runs for a sequence of values and thus determine the optimum SOL depths 'by hand'.

It was considered desirable to make the choice of spline parameters as intuitive as possible. This was achieved by defining the basis spline at each knot as the (unique) interpolating spline which is valued at unity at that knot and zero at all other knots included in the parameterization. The *Numerical Recipes* routine SPLINE was used to calculate these splines. Fig. 1 shows the individual spline basis functions and the sum of all 4 splines for the example of 3 internal knots at $1 - \hat{\psi} = 0.25, 0.50, 0.75$. These functions are oscillatory, it is true, but the oscillations die away exponentially and, discounting the oscillations, these basis functions are

Fig.1 Spline basis functions for knots at {0.0,0.25,0.50,0.75,1.0} (with symbols ) and their sum (without symbols )

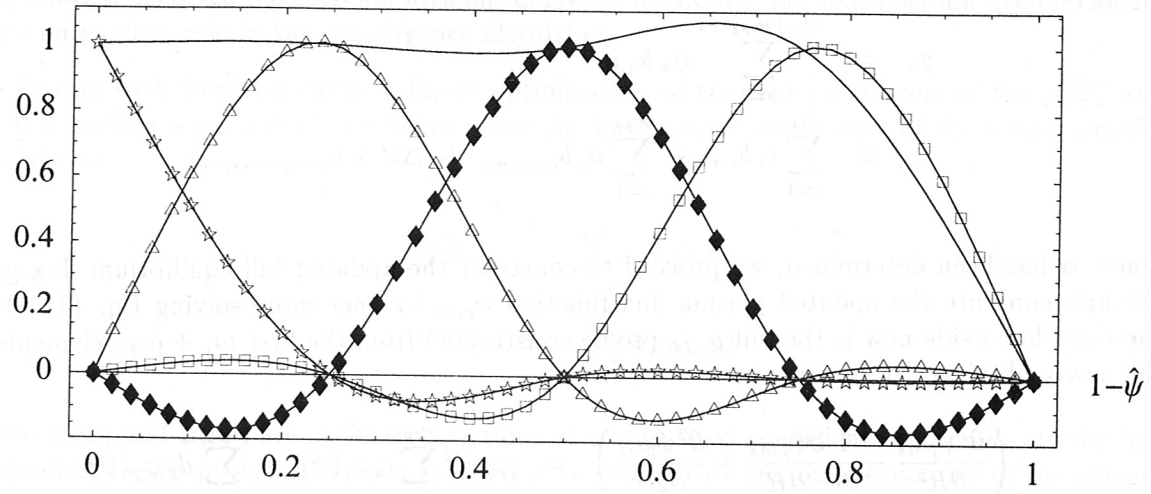


Fig. 2(a) First four splines for knots at {0,0.25,0.50,0.75,0.90,0.95,0.98}

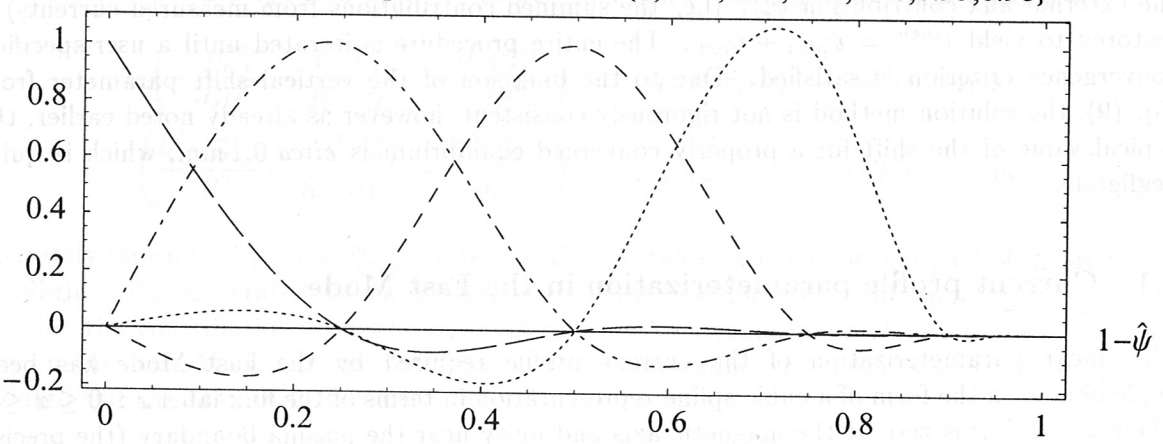


Fig. 2(b) Last 3 splines for knots at {0,0.25,0.50,0.75,0.90,0.95,0.98} (non−solid ) and weighted sum of all seven splines (solid line )

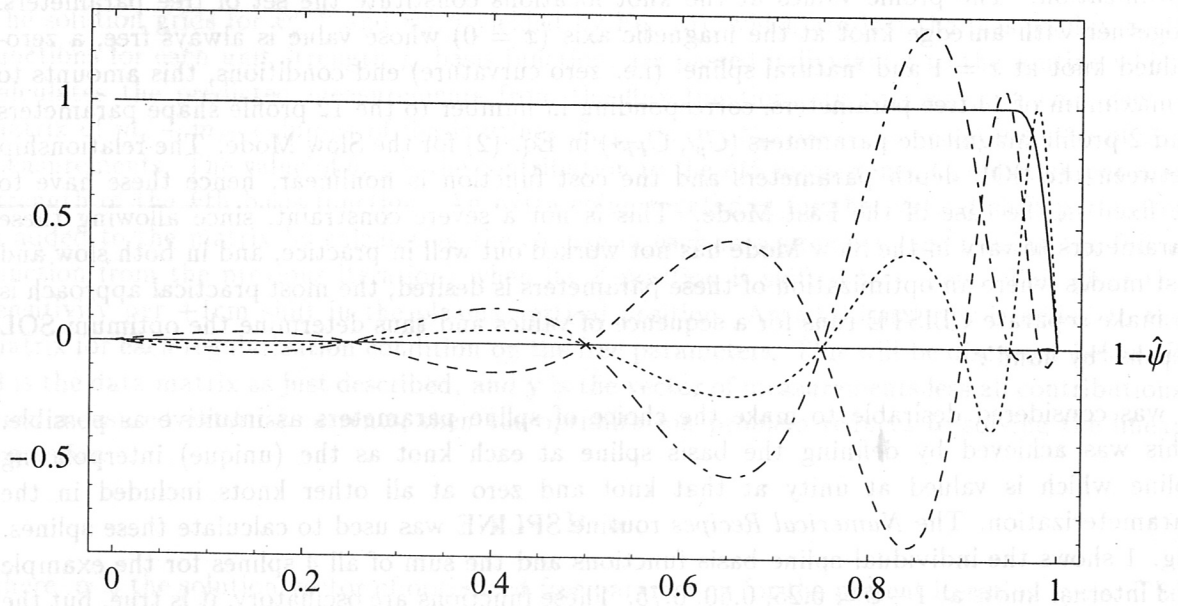

much more localized than the well-known cubic 'B-Splines' which stay above zero over a span of 5 knots (outside this region, however, they are zero everywhere, in contrast to the choice made here). Figs. 2(a) and 2(b) shows corresponding plots for the internal knot sequence $\hat{\psi} = 0.25, 0.50, 0.75, 0.90, 0.95, 0.98$. Here the behaviour of the individual basis functions becomes strongly oscillatory near the edge, but note that we can still construct flat profiles using this basis. The solid curve in Fig. 2(b) is a linear combination of the 7 splines (i.e. the 6 internal splines plus the spline passing through (0,1)) with the vector of weights: {1,1,1,1,1,1,0.743}. It has almost zero curvature over the range $0 \leq \hat{\psi} \leq 0.95$.

These basis splines are our choice for the $\pi_i(\psi)$ and $\varphi_j(\psi)$ basis functions in Eq. (4) above.

It is also possible to use a polynomial parameterization of the source profiles, where the 6 internal knot parameters are now reinterpreted as powers of $\hat{\psi}$ ranging from 0 (i.e. a constant offset) to 5. The knot positions play no role in this choice of parameterization.

### 3.2 Regularization of the current profile in the Fast Mode

To guard against unstable results when the available measurements may not justify the number of free parameters in the current profile parameterization, regularization in the form of a curvature penalty may be selected by the user. This is achieved by adding $m_p + m_{FF}$ additional rows to the **B** matrix, consisting of the (weighted) second difference of the $p'(\psi)$ or $FF'(\psi)$ profile evaluated in turn at the knot position of each free parameter. Each row is a linear combination of the as yet undetermined free parameters involving at most three adjacent knot values and is a (weighted) discrete approximation to the curvature, at that knot position, of the $p'(\psi)$ or $FF'(\psi)$ profile. For each such additional row, the **y** vector of measurements is augmented by a zero-valued element, corresponding to a target curvature of zero. It is not difficult to show that this approach leads to the same solution vector $\boldsymbol{\alpha}$ as that obtained from the apparently more compact representation of the optimization problem with a single discretely calculated curvature penalty term:

$$\text{Cost} = \sum_{n=1}^{N_m} \left( y_n - \sum_{j=1}^{m_p+m_{FF}+1} \alpha_j \, b_{n,j} \right)^2 + \lambda \left( \sum_{k=1}^{m_p} p'''(\psi_k)^2 + \sum_{k=1}^{m_{FF}} FF'''(\psi_k)^2 \right) \qquad (10)$$

where augmentation of **y** and **B** has been avoided. Moreover, the regularization scheme employed here allows individual weighting of the curvature contribution at each knot to fine-tune the regularization. This is particularly useful where there is a physics-based expectation that the curvature may be naturally high for certain regions of the profile e.g. as in the case of strong bootstrap current.

## 4 Running Sequence

The following outline indicates the sequence of steps necessary to run CLISTE to interpret a set of experimental measurements.

### 4.1 Preparing Input Data

Before CLISTE can be run, the shot data to be fitted must be obtained and prepared. As described above, CLISTE requires the poloidal field currents as well as the toroidal magnetic field (the latter to scale the $q$-profile correctly). The magnetic measurements consist of a set

of magnetic field pickup coils and flux differences (from both $2\pi$ flux loops and saddle loops) which, for ASDEX Upgrade, are all available from the level 0 shotfiles MAG,MAI and MAD. In addition to these measurements, the values of 96 scalar plasma parameters calculated by the FP algorithm [8] FPG are read in for comparison with the equivalent CLISTE parameters. In the prepare step, (executed by a dedicated `prepare` script) all these data are accumulated from different diagnostics for a particular shot and a specified time-window and time-slices. The data are synchronized in time and stored as ASCII datafile #####.fmp, which can be read by CLISTE via scripts as a whole or piecewise.

When CLISTE requests additional input from other diagnostics e.g. MSE, a time-synchronized file #####.mse is also generated.

### 4.2 User Specified Input Parameters

Once the diagnostic data for the specified shot number and time(s) has been prepared by the `prepare` script, the user has the option of making detailed choices with regard to the selection and weighting of signals, the current density profile parameterization and other features. Apart from the choice of grid resolution, which is specified in the `standard.augd` input file, all user choices are made in the `flags` file; either the default `standard.flags` or, if it has been created by, e.g., copying `standard.flags` and customizing it, the shot-specific `#####.flags`. We do not offer here an individual description of the 438 different fields (as of April 1999) in this file, referring the reader instead to a user-friendly menu system which describes and allows alteration of these parameters, which is currently under development.

### 4.3 Running CLISTE

Using the above data together with data files defining the ASDEX geometry and the numerical parameters for the equilibrium and CLISTE calculations, CLISTE can be run for one or more timesteps of a particular shot. Different timeslices (or time-windows) may alternatively be run on different Unix systems and/or in parallel on different workstations. An easy to use unix script initiates the generation of input files and controls and records the calculation sequence as well. In addition, a window shell script enables a simple default use of the code with some standardized input parameter decks. The nomenclature of files, consisting of shotnumber, time and a runnumber, support an easy reference to analyzed shots. The typical CPU-time to analyze a single time step is about 8 seconds for a $65 \times 129$ grid on a Sun sparc ultra 300 MHz workstation. The present size of the code (which allows a maximum grid resolution of $257 \times 257$) is about 45 Mbyte.

## 5 Output Data

Each CLISTE run (i) produces results in graphical and text form, (ii) optionally saves converged equilibria to disk ('eqDSK' files), and (iii) generates a log file with details of the convergence history and other ancillary information. For successful runs, the eqDSK-files can be used to write a higher level shotfile EQI with up to 75 timeslices (equilibria) for a particular shot. These shotfiles can be further used for mapping procedures (e.g. rhopol $\rightarrow$ rhotor, etc.), for generating grids for further calculations (scrape-off modelling, B2-Eirene), or stability calculations. Since the format of the generated shotfiles EQI are identical with other equilibrium results of AUGD, like EQA, EQU, FPP, all subsequent calculations can readily use CLISTE results.

Figure 3: Poloidal flux contour plot, current density and pressure mid-plane profiles, and parameters of the equilibrium (text) for ASDEX Upgrade # 11722, t= 3.101 s. The black dots joined by dot-dashed lines represent flux loop pairs and the open boxes are magnetic probes.

A sample CLISTE Fast Mode equilibrium, for ASDEX Upgrade discharge # 11722, $t = 3.101$ s is shown in Fig. 3. It includes a flux surface contour plot, the toroidal current density profile $j_\phi(R, Z_{mag})$ and equilibrium pressure profile $p(R, Z_{mag})$ along the horizontal chord through the magnetic axis, and text showing the values of leading input data and output plasma parameters. The key to the text information is as follows:

```
CLISTE Fast Equilibrium AUG # 11722 t  3.101 Ip  0.800 MA  Bo -2.4647 T
```

- Shotnumber, time, plasma current, vacuum toroidal field at $R = 1.65$ m.

```
   V1o    V1u     V2o    V2u     V3o    V3u    CoIo   CoIu    OH
 0.749  1.838  -0.200 -0.874  -0.204 -0.225  -0.004  0.004  -7.418 MA
  8.05  19.76   -2.33 -10.17   -7.30  -8.02   -0.79   0.80 -10.877 kA
Ipslo  Ipslu   pslqo  pslqu    OH2o   OH2u
 0.002  0.003   0.000  0.000   0.000  0.773 MA
  1.86   2.53    0.00   0.00    0.00   9.55 kA
```

- The above are the fitted poloidal field coil currents which, for the Fast Mode, coincide exactly with the measured currents. The MA data give the total Ampere-Turns through each coil group, the kA data give the 'winding current', i.e. the current per turn.

```
R,Zmag ( 1.665,  0.126) R,Zcur ( 1.640,  0.119) R,Zgeo ( 1.606,  0.087)
```

- Coordinates of the magnetic axis, current centroid, and area-weighted geometric centroid.

```
a 0.517 b 0.831 k 1.610 ko 1.240 D  0.066 A  1.333 V   13.45
```

- Horizontal `a` and vertical `b` minor radii (area weighted), Elongation (`k=b/a`), Elongation at magnetic axis `ko`, Triangularity `D`, Area `A`, Volume `V`.

```
Rin 1.089 Rout 2.147 Ztop 0.908 Zbot -0.868 Fstab,Fun  0.78   0.66 MN/m
```

- Minimum `Rin` and maximum `Raus` R-values on plasma boundary, maximum `Ztop` and minimum `Zbot` Z-values on plasma boundary. Stabilizing `Fstab` and destabilizing `Fun` force gradients on plasma.

```
Knots 0.300 0.400 0.600 0.800 0.900 0.950
```

- Positions of 6 internal knots on the $1 - \hat{\psi}$ axis for parameterizing $p'(\psi)$ and $FF'(\psi)$. Note the subset of internal knots actually used ($0 \leq n_{knots} \leq 6$) is specified in the `flags` file.

```
C8 0.211 Pd  0.000  0.000  0.000  0.000 \fd  0.482  0.000  0.000  0.000
BootP  0.000  0.00 \f  0.000  0.00 c0p,\f   0.202   3.505 Ipres   19.9%
```

- Current profile parameters: The first parameter (= 0.211) is an independent input parameter for the Slow Mode, but is a dependent parameter for the Fast Mode. It is smaller than $\beta_{pol}$ by the ratio $(\int_{\partial\Omega} dl)^2/4\pi A$ where $\int_{\partial\Omega} dl$ is the circumferunce of the plasma boundary and $A$ is the cross-sectional area. For a circular plasma shape, the ratio is unity. The next two groups of 4 parameters on the first line (following the labels `Pd` and

FFd) are the normalized profile values at the positions of the first four knots in the $p'(\psi)$ and $FF'(\psi)$ profiles, respectively. The normalized profile values at the remaining 2 knot positions for each profile are labelled Bootp (for $p'$) and FF (for $FF'$) on the second line. These results are presented in normalized form, $\hat{p}'(\hat{\psi})$ and $\hat{FF}'(\hat{\psi})$, where $\hat{p}'$ and $\hat{FF}'$ are each unity on the magnetic axis. *Any zero-valued parameter indicates that the particular knot was not included for that profile.* Thus, for the present example, no internal knots were used in the $\hat{p}'(\psi)$ profile, which therefore reduces to the straight line valued at unity on the magnetic axis and zero at the plasma boundary (and hence to an approximately parabolic spatial profile). Just one internal knot (the first, at $x = 1 - \hat{\psi} = 0.300$) was included in the $\hat{FF}'(\psi)$ profile and the fitted value is 0.482. The scale factors c0p and c0FF convert normalized to absolute profiles , i.e. $p'(\hat{\psi}) = c0p \times \hat{p}'(\hat{\psi})$ etc. These factors correspond to $C_{p'}$ and $C_{FF'}$ in the Slow Mode profile parameterization discussed earlier. Ipres gives the percentage toroidal current driven by the $p'(\psi)$ profile.

```
dSOLp,f 0.0000 0.0000Vs Isol 0.000 0.000kA Jax,Jxp 2.442 0.000MA
```

- Scrape-off layer parameters: dSOLp,FF show the magnetic depths, in the 'public' scrape-off region, of the $p'$ and $FF'$ profiles. The 'private region' depths are usually chosen to be 50% of the corresponding public values. Isol gives the currents flowing in the 'public' and 'private' scrape-off regions, respectively. Jax,Jxp give the current densities on the magnetic axis and x-point. The latter is zero unless dSOLp or dSOLf exceeds zero.

```
bpol 0.248 Li 1.377 Qo 0.978 Q95  5.098 Fax-Fb   1.51Vs Wmhd    0.105 MJ
```

- $\beta_{pol}$, $l_i$, $q_{axis}$, $q_{95\%}$, $\psi_{axis} - \psi_{boundary}$, plasma energy content.

```
Xpt( 1.494, -0.868) Fb-Fx  0.000 Vs Xp2( 1.625,  1.269) Fb-Fx  0.210 Vs
```

- $(R, Z)_{\text{x-pt}}$ and $\psi_{boundary} - \psi_{\text{x-pt}}$ for the x-point nearest and second-nearest, respectively, to the plasma boundary. In the case of an x-point plasma (in contrast to a limiter plasma), the first x-point will lie on the plasma boundary.

```
ILp( 1.051,  0.196) Fb-Fl  0.109 Vs OLp( 2.131,  0.512) Fb-Fl  0.156 Vs
```

- $(R, Z)_{limiter}$ and $\psi_{boundary} - \psi_{limiter}$ for the inboard limiter and outboard (ICRH antenna) limiter points nearest the plasma boundary.

```
i:  11 <dF>   1.5mT  2.3% <dB>   1.4mT  0.7%  <deg> 0.00 Cost   0.0924
```

- Fit statistics: i: gives the number of iterations to convergence. (For the Slow Mode, i: gives the number of calls to the GEC.) <dF> is the rmse fit error for magnetic flux difference measurements. These are converted to field values by normalizing each flux to the area spanned by the two flux loops across which the flux difference is measured. The adjacent percentage is this rms error expressed as a percentage of the rms value of all the converted flux differences. <dB> is the rmse fit error for magnetic probe $B_\theta$ measurements. The adjacent percentage has the same significance as that following the <dF> value. <deg> gives the rms fit error in degrees for MSE channels used in the fit. A zero error indicates that none were used here. Cost gives the final value of the Cost function, i.e. the sum of squared residuals for all non-zero weighted measurements and other factors such as curvature penalties that constrained the interpretation.

The horizontal axis for current density and pressure profiles covers the range $1.00 \leq R \leq 2.20$ and the short vertical marks below the $R-$axis denote where the profiles intersect the plasma boundary. The dashed vertical line above the $R-$axis marks the magnetic axis position. The dot-dashed curves above and below each solid profile are one standard deviation (approx. 65%) confidence bands for the fitted profiles, whose calculation method and interpretation is next considered.

### 5.1 Calculation of Error Bars and Profile Confidence Bands

The starting point for calculation of error bars for individual scalar parameters and confidence bands for plasma profiles is the $N \times N$ variance-covariance matrix **Vmat** of the $N$ fitted parameters $\alpha_i$, $_{(i=1...N)}$ which is returned by the linear regression routine in the case of the Fast Mode, or by calling the auxillary Nag routine `E04YCF` subsequent to the main minimization routine `E04FCF` in the case of the Slow Mode. The diagonal of this matrix holds the variances, i.e. squared standard deviations, for the fitted parameters, while the off-diagonal terms hold the covariances.

If $g$ is any parameter of the interpreted equilibrium and $\nabla_{\boldsymbol{\alpha}} g$ is the gradient vector of $g$ with respect to the set of fitted parameters $\alpha_i$, then the standard deviation in $g$, $\sigma_g$, is given by:

$$\sigma_g^2 = \nabla_{\boldsymbol{\alpha}}^t g \cdot \mathbf{Vmat} \cdot \nabla_{\boldsymbol{\alpha}} g \tag{11}$$

For spatial profiles (as a function of $R$, say) confidence bands can be constructed in a pointwise manner by treating each element of a regularly spaced array of profile values as a separate parameter and interpolating the calculated array of standard deviations to form a continuous function $\sigma(R)$. In the Slow Mode, the calculation of the gradient vector $\nabla_{\boldsymbol{\alpha}} g$ is relatively expensive, since the GEC must be called at least once for each free parameter (which yields a forward difference with respect to the converged solution value for each $g$ whose error bar is sought; a centred difference would require two calls to the GEC per free parameter). The calculation can be performed very efficiently, however, in the Fast Mode provided the parameter gradients can be related to the $j_\phi$ basis functions. This is the case, clearly, for the $j_\phi$, $p'$ and $FF'$ profiles. For the $j(R)$ profile, for example, we have from Eqs. (3- 5) that

$$j_\phi \;=\; R\sum_{i=1}^{m_p} c_i\,\pi_i(\psi) \;+\; \frac{1}{\mu_o R}\sum_{j=1}^{m_{FF}} d_j\,\varphi_j(\psi) \tag{12}$$

Thus, knowing $\psi(R,Z)$ from the converged equilibrium flux grid, we have

$$\nabla_{\boldsymbol{\alpha}}\, j_\phi(R,Z) = \left[R\,\pi_1(\psi(R,Z)),\ \ldots,\ R\,\pi_{m_p}(\psi(R,Z)),\ \varphi_1(\psi(R,Z))/\mu_o R,\ \ldots,\ \varphi_{m_{FF}}(\psi(R,Z))/\mu_o R\right]$$

i.e. to calculate $\nabla_{\boldsymbol{\alpha}}\, j_\phi(R,Z)$ and hence the confidence band for the $j(R,Z_{mag})$ profile, we simply evaluate the basis functions at regular intervals along the horizontal chord using the last expression.

For an arbitrary profile which is a flux function $s(\psi)$, say, a more general approach is required. We first note that the gradient profile (with respect to the fitted parameters) for any $s(\psi)$ may be written as

$$\nabla_{\boldsymbol{\alpha}}\, s(\psi) \;=\; s'(\psi)\nabla_{\boldsymbol{\alpha}}\,\psi \tag{13}$$

where $s'(\psi) = ds(\psi)/d(\psi)$. Now for each $j_\phi$ basis function $\pi_i(\psi)$ or $\varphi_j(\psi)$, the mid-plane profile of the corresponding basis flux function $\psi_{p,i}(R,Z_{mag})$ or $\psi_{FF,j}(R,Z_{mag})$ is stored by the code. From Eq. (6) it is easy to see that these are precisely the gradient profiles $\nabla_{c_i}\,\psi$ and $\nabla_{d_j}\,\psi$ that we require to evaluate Eq. (13) and hence calculate confidence bands for any flux function.

Figure 4: ASDEX Upgrade # 11722, t=3.101 s with one free shape parameter in the pressure profile parameterization. Only the pressure magnitude was free in Fig. 3.

It is important to note that error bars obtained by the above procedure are specific to the choice of current profile parameterization, curvature penalty, etc., and hence cannot be regarded as objectively 'correct'. They are, however, useful for identifying the minimum adequate number of free parameters in the model. In particular, if the error bounds for a given profile are excessive, this indicates that the profile has too many free parameters and can be further regularized. The model for $j_\phi$ used to find the equilibrium shown in Fig. 3 has only 3 free parameters (the two scale factors `c0p`, `cOFF` and a free knot value in the $FF'(\psi)$ profile), however adding a fourth free parameter is already overfitting the pressure profile, as can be seen from Fig. 4, where the addition of a free internal knot to the $p'(\psi)$ profile resulted in substantially increased error bars on the $p(\psi)$ profile, while the improvement in the Cost function was negligible (0.0922 versus 0.0924). On the other hand, the current profile is still strongly regularized since the small uncertainty in the current density on the magnetic axis is unrealistic, given the absence of MSE or other data sensitive to the poloidal field inside the plasma. The conclusion from this example is that the available constraints on the interpretation problem, namely the external magnetic measurements, are sufficient to identify the integral of the pressure profile but contain no information to identify its shape.

## 6 Acknowledgments

The first author is most grateful to Karl Lackner for illuminating discussions at critical junctures in this work and for his continuing support. A particular debt of gratitude is due to Wolfgang Zwingmann, now at Cadarache, who provided the critical insight into the essence of the EFIT algorithm during a visit by the first author to JET in September 1998. Fruitful discussions with Josef Neuhauser, Simon Pinches (who wrote the first version of CLISTE documentation) and Hans-Peter Zehrfeld are also cordially acknowledged.

## References

[1] V. D. Shafranov, Sov. Phys. JETP **6**, 545 (1958); Zh. Eksp. Teor. Fiz. **33**, 710 (1957).

[2] H. Grad and H. Rubin, in *Proceedings of the Second United Nations Conference on the Peaceful uses of Atomic Energy* (United Nations, Geneva, 1958), Vol. 21, p. 190.

[3] K. Lackner, Comput. Phys. Commun. **12** 33 (1976).

[4] Numerical Algorithms Group.

[5] D. M. Bates, (1988) *Nonlinear regression analysis and its applications*, Wiley, New York, 85.

[6] L.L. Lao, Nucl. Fusion **25** 1611 (1985).

[7] J.R. Ferron, Nucl. Fusion **38** 1055 (1998).

[8] P.J. Mc Carthy, Ph.D. thesis, University College Cork, 1992.